

Sub-percentage measure of distances to redshift of 0.1 by a new cosmic ruler

Yong Shi,^{1,2*} Yanmei Chen,^{1,2} Shude Mao,^{3,4} Qiusheng Gu,^{1,2} Tao Wang,^{1,2} Xiaoyang Xia,⁵ Zhi-Yu Zhang.^{1,2}

¹*School of Astronomy and Space Science, Nanjing University, Nanjing 210093, China.*

²*Key Laboratory of Modern Astronomy and Astrophysics (Nanjing University), Ministry of Education, Nanjing 210093, China.*

³*Department of Astronomy, Tsinghua University, Beijing 100084, China.*

⁴*National Astronomical Observatories, Chinese Academy of Sciences, 20A Datun Road, Chaoyang District, Beijing 100012, China.*

⁵*Tianjin Astrophysics Center, Tianjin Normal University, Tianjin 300387, People's Republic of China.*

Accepted XXX. Received YYY; in original form ZZZ

ABSTRACT

Distance-redshift diagrams probe expansion history of the Universe. We show that the stellar mass-binding energy (massE) relation of galaxies proposed in our previous study offers a new distance ruler at cosmic scales. By using elliptical galaxies in the main galaxy sample of the Sloan Digital Sky Survey Data Release 7, we construct a distance-redshift diagram over the redshift range from 0.05 to 0.2 with the massE ruler. The best-fit dark energy density is 0.675 ± 0.079 for flat Λ CDM, consistent with those by other probes. At the median redshift of 0.11, the median distance is estimated to have a fractional error of 0.34%, much lower than those by supernova (SN) Ia and baryonic acoustic oscillation (BAO) and even exceeding their future capability at this redshift. The above low- z measurement is useful for probing dark energy that dominates at the late Universe. For a flat dark energy equation of state model (flat w CDM), the massE alone constrains w to an error that is only a factor of 2.2, 1.7 and 1.3 times larger than those by BAO, SN Ia, and cosmic microwave background (CMB), respectively.

Key words: galaxies: general; galaxies: kinematics and dynamics; cosmology: observations; cosmology: cosmological parameters

1 INTRODUCTION

A distance-redshift diagram is a powerful probe of the cosmic expansion history. The measurement by E. Hubble and G. Lemaître revealed the expansion of the Universe (Hubble 1929; Lemaître 1927), laying down the foundation of the big bang theory. In the past decades, two independent distance rulers at cosmic scales with appreciable redshifts, supernova Ia (SN Ia) and baryonic acoustic oscillation (BAO), demonstrated unambiguously the acceleration of the cosmic expansion, implying the existence of dark energy (Riess et al. 1998; Perlmutter et al. 1999; Eisenstein et al. 2005).

It is essential to have independent rulers to measure the distance vs. redshift diagram. Physically, different rulers probe the cosmic geometry from different aspects, thus examining a concordant cosmological model. Technically, each ruler has “nuisance” parameters that are unrelated to the cosmological parameters but can introduce systematic errors (e.g. Zuntz et al. 2015). Joint analysis by combining different rulers can significantly alleviate the degeneracy among cosmological parameters and improve their accuracy.

Uncertainties of current distance measurements using SN Ia and BAO are around a few percent and vary with redshift, mainly limited by the sample size and survey volume (Ross et al. 2015; Alam et al. 2017; Scolnic et al. 2018). In the forthcoming 5–10 years, large

imaging and spectroscopic surveys will reach precision from a few sub-percent to one percent per redshift bin of 0.1 (Feng et al. 2014; DESI Collaboration et al. 2016). In this letter, we show that the relation between stellar masses and binding energies of galaxies as proposed in Shi et al. (2021) offers distance rulers at cosmic scales with significant statistical power. Through the study we will refer this relation as massE where “mass” stands for stellar masses and “E” for binding energies.

2 THE MASSE COSMIC RULER

Shi et al. (2021) demonstrated a tight relation between stellar mass and binding energy of galaxies, which covers nine orders of magnitude in stellar masses over a large range of galaxy types and redshift. The overall relationship is described by double power laws with the transition galaxy stellar mass of $\sim 10^7$ – $10^8 M_\odot$. As illustrated in their Fig. 2 and 3, the dependence on redshift is absent up to $z \sim 2.5$, so does the dependence on galaxy properties such as galaxy sizes, surface densities and star formation rates. The physical origin of the massE relation may be related to the self-regulation of a galaxy between its binding energy and the accumulative feedback energy from its stellar populations. Although the massE relation holds for various types of galaxies, in this study we only use elliptical galaxies so that the velocity dispersion can be measured through single fibers.

* E-mail: yshipku@gmail.com

For galaxies with stellar masses well above $10^8 M_\odot$, the massE relation can be written as a single power law:

$$\sigma_e R_e^{0.25} = A M_{\text{star}}^\beta, \quad (1)$$

where R_e is the effective radius that encloses half of stellar light, M_{star} is the total stellar masses of galaxies, σ_e is the velocity dispersion within R_e for dispersion-dominated galaxies, and $\beta=0.4036\pm 0.0016$ (see § 3). $\sigma_e R_e^{0.25}$ represents the fourth root of the galaxy binding energies within R_e .

In Equation 1, σ_e is independent of redshift, $\frac{R_e}{\text{kpc}} = \frac{R_{e,\text{as}}}{206.27} \frac{D_A}{\text{Mpc}}$ and $M_{\text{star}} = M_{\text{star},1\text{Mpc}} \left(\frac{D_L}{1\text{Mpc}}\right)^2$, where $R_{e,\text{as}}$ is the apparent effective radius in arcsec, $M_{\text{star},1\text{Mpc}}$ is the galaxy stellar mass placed at a distance of 1 Mpc, the angular diameter distance D_A is related to the luminosity distance D_L in $D_A = D_L / (1+z)^2$. $M_{\text{star},1\text{Mpc}}$ can be obtained by first redshifting the observed spectral energy distribution (SED) to the rest-frame and then fit with stellar population synthesis models to obtain the mass-to-light ratio and the corresponding mass at a distance of 1 Mpc. $M_{\text{star},1\text{Mpc}}$ is essentially a flux-like quantity and its measurement is independent of cosmological models.

As a result, the corresponding angular diameter distance calculation is:

$$\frac{D_A}{\text{Mpc}} = S_{D_0} \frac{D_0}{\text{Mpc}} \left[(1+z)^{-4\beta} \frac{\sigma_e}{\text{km s}^{-1}} \left(\frac{M_{\text{star},1\text{Mpc}}}{M_\odot}\right)^{-\beta} \left(\frac{R_{e,\text{as}}}{\text{arcsec}}\right)^{0.25} \right]^{1/(2\beta-0.25)}, \quad (2)$$

with $D_0 = \left(\frac{0.264 \text{ km s}^{-1} \text{ kpc}^{0.25} M_\odot^{-1}}{A}\right)^{1/(2\beta-0.25)}$ in Mpc. When applying Equation 2 to estimate distances for cosmological purpose, the exact D_0 always degenerates with the local Hubble constant H_0 , similar to the case of the absolute magnitude of SN Ia. As a result, a nuisance parameter S_{D_0} is included as the scaling factor for a sample to reproduce the local Hubble constant, and is related to the absolute calibration of three observables (σ_e , $M_{\text{star},1\text{Mpc}}$, $R_{e,\text{as}}$). The second nuisance parameter β can be estimated from local samples as detailed in § 3.

Not that although the massE relation invokes the same three observables as the fundamental plane, they are different both physically and quantitatively. As shown in Shi et al. (2021), the massE is a correlation between galaxy stellar masses and binding energies while the fundamental plane is between galaxy stellar mass and dynamical masses. For galaxies above $10^8 M_\odot$, the massE relation only has two free parameters that are A and β in Equation 1, while the fundamental plane has three free parameters that are a , b and c in Equation 5 of Shi et al. (2021). Furthermore, it has been known that the fundamental plane needs a fourth hidden systematic parameter to account for the dependence on galaxy properties or local environments (e.g. Bernardi et al. 2003; Magoulas et al. 2012; Howlett et al. 2022). As a result, the fundamental plane is mainly limited to $z < 0.05$ -0.1 for peculiar velocity studies (e.g. Howlett et al. 2022).

The following strategy is proposed to measure the distance vs. redshift diagram using the massE cosmic ruler. For a selected sample in a given redshift bin, its median redshift, if ignoring the peculiar velocity, corresponds exactly to its median luminosity distance, because the luminosity distance increases monotonically with redshift, independent of cosmological models. As a result, we measure the median of the redshift distribution and the median of the luminosity distance distribution in individual redshift bins to obtain the distance vs. redshift diagram. With this strategy, the sample incompleteness does not matter, i.e., objects rejected by the selection function does not affect at all the correspondence between the median distance and median redshift. But the Malmquist bias does matter in a way that,

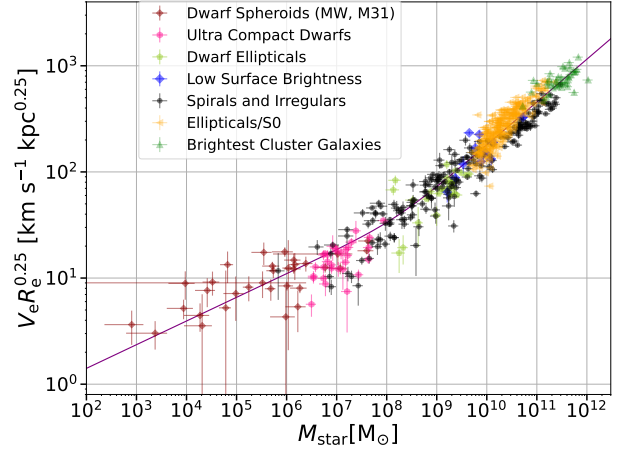


Figure 1. The local sample compiled in Shi et al. (2021) that is used to derive the intrinsic massE relationship. V_e is rotation velocity and velocity dispersion for rotation dominated and dispersion dominated galaxies, respectively. For details, see Shi et al. (2021). The solid line indicates the derived intrinsic relationship after considering errors on both X and Y axes (see § 3).

e.g., a sample with a magnitude cut is intrinsically fainter so that their stellar mass is over-estimated.

3 THE MASSE RELATIONSHIP OF THE LOCAL SAMPLE

Before applying the massE to the SDSS sample, we first need to estimate the intrinsic massE relationship, especially β in Equation 1. We thus perform the fitting to the sample compiled and homogenized in Shi et al. (2021), while excluding luminous infrared galaxies and ultra diffuse galaxies because of their large observational errors as well as high- z sources in order to remove the dependence of the relationship on the cosmological model. This local sample contains 589 objects as shown in Fig. 1. Measurements of galaxy sizes, velocity dispersions and stellar masses of the sample in general have high signal to noise. We thus add additional 0.1 dex, 10% and 1% systematic errors quadratically to M_{star} , R_e and σ_e , respectively. The systematic error for M_{star} is mainly caused by uncertainties in population synthetic modeling, which can be illustrated by comparing the MPA-JHU and CIGALE stellar masses of SDSS galaxies in § 6.1. The uncertainty for R_e is from background subtraction, morphology irregularity, galaxy center determination etc. We estimated this by selecting a subsample of SDSS galaxies with high R_e signal-to-noise ratio > 100 and comparing measurements from different data releases. The systematic error for σ_e is mainly caused by absolute wavelength calibration and 1% is a reasonable estimate for modern CCD-based spectra (Law et al. 2021). If increasing the errors by a small amount, e.g., to 0.15 dex for M_{star} , to 15% for R_e and to 2% for σ_e , respectively, the difference in the derived slope β is within one σ .

We performed PyMC3 (Salvatier et al. 2016) by considering errors on both M_{star} and $\sigma_e R_e^{0.25}$ to obtain the intrinsic relationship. The best fit gives $\beta=0.4036\pm 0.0016$ and the corresponding D_0 co-varies with β through:

$$\ln(D_0/\text{Mpc}) = (26.06\beta - 5.54) \pm 0.005. \quad (3)$$

The derived slope β is similar to that in Shi et al. (2021) but with a smaller error, because in Shi et al. (2021) the fitting was done without weighting by observational errors, which thus gives the result including the observational error instead of the intrinsic relationship.

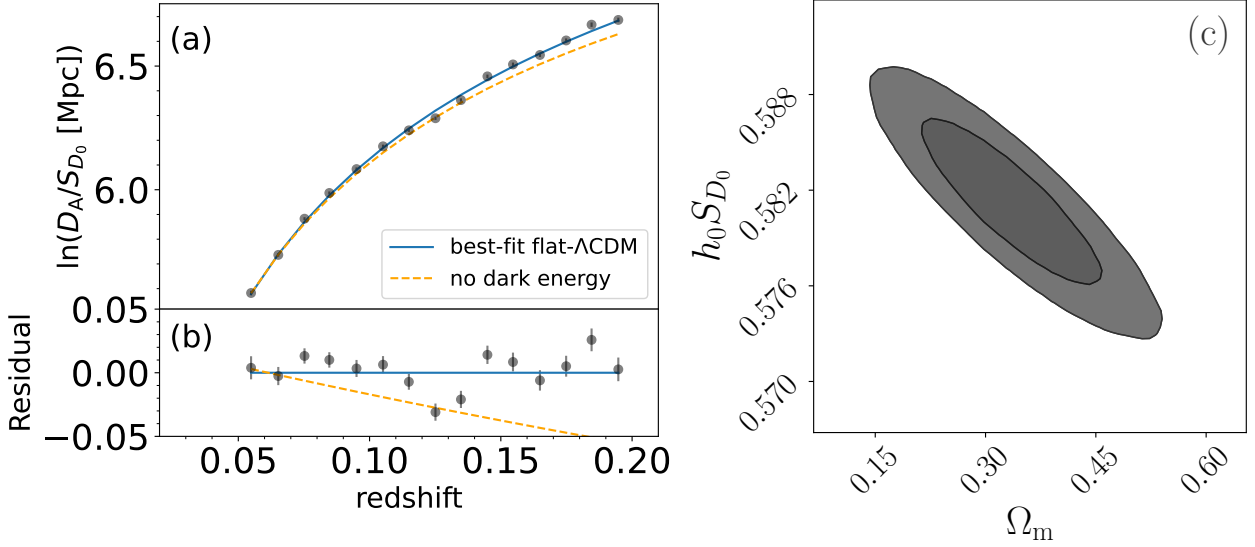


Figure 2. (a) The distance vs. redshift diagram that is derived from elliptical galaxies in the SDSS main galaxy sample using the massE ruler. D_A is the angular-diameter distance in Mpc and S_{D_0} is the scale factor that calibrates the absolute distance and degenerates with local Hubble constant. The error bars indicate the square root of the diagonal elements of the covariance matrix shown in in Figure 3 (a). The solid line represents the best-fit flat Λ CDM with $\Omega_\Lambda=0.675\pm 0.079$. The dashed line is the one without dark energy normalized at two lowest-redshift bins. (b) The residual of the best fit. As shown in § 6.2, the scatter in the residual is consistent with the covariance matrix in Figure 3 (a). (c) The confidence ranges of dark matter density (Ω_m) and the product $h_0 S_{D_0}$ at 68% and 95%, where h_0 is the local Hubble constant in 100 km/s/Mpc. The plot was produced through ChainConsumer (Hinton 2016).

Distances of this local sample are mostly below 40 Mpc, with the remaining 17% of the sample distributes between 40 and 300 Mpc. They are mainly based on cosmological-independent measurements for those below ~ 20 Mpc, but are homogenized to a flat Λ CDM with $H_0=73$ km/s/Mpc, and $\Omega_\Lambda=0.73$ for those above 20 Mpc. However, the best-fit β changes only by a small fraction of its $1\text{-}\sigma$ error if changing to $\Omega_\Lambda=1.0$ or $\Omega_\Lambda=0.4$, respectively. This is because the associated change in R_e and M_{star} is much smaller than their observational errors, plus the fact that both X and Y-axes vary simultaneously to partially cancel out the effect.

We also carry out additional fitting to the massE relationship by including 105 high- z objects compiled in Shi et al. (2021). The derived $\beta=0.4045\pm 0.0016$ is essentially the same as the one with only the local sample. This suggests that β should not evolve strongly with the redshift.

4 ELLIPTICAL GALAXIES IN THE MAIN GALAXY SAMPLE OF SLOAN DIGITAL SKY SURVEY (SDSS)

Although all types of galaxies can be used for the massE ruler, elliptical galaxies are the most suitable ones given their low extinction, regular morphologies, low current star formation rates and dispersion dominated kinematics, which will facilitate measurements of three observables (σ_e , $M_{\text{star},1\text{Mpc}}$, $R_{e,\text{as}}$). Unlike spiral galaxies whose velocity requires spatially-resolved kinematic maps, ellipticals’ can rely on single-fiber measurements (Cappellari et al. 2006; Shi et al. 2021). We build our elliptical galaxy sample from the value-added MPA-JHU catalog (Kauffmann et al. 2003; Brinchmann et al. 2004) of the SDSS data release 7¹. A sample of about 28,000 elliptical galaxies were selected from the SDSS main galaxy sample with the following criteria: (1) no redshift warning as indicated by $Z_WARNING=0$; (2) the main galaxy sample as defined by

$\text{PRIMTARGET} \geq 64$ but < 128 and Petrosian magnitude in $r \leq 17.77$; (3) elliptical galaxies as defined by $\text{FRACDEV} \geq 0.8$. Only the second criterion will introduce the Malmquist bias while others are not related to the three observables (σ_e , $R_{e,\text{as}}$, $M_{\text{star},1\text{Mpc}}$).

To apply Equation 2, we adopt the Petrosian radius in the r band (PETROR50_R) to represent R_e . The total stellar mass M_{star} adopts MSTAR_TOT that is derived from fitting to Petrosian magnitudes in four SDSS optical bands. The advantage of the Petrosian radius and magnitude is that there is no bias in redshift due to the surface dimming (Blanton et al. 2001), which is the key for the distance vs. redshift measurement. M_{star} is converted to $M_{\text{star},1\text{Mpc}}$ simply through the adopted cosmology for the MPA-JHU catalog.

We carry out our own measurements of the velocity dispersion, because those in the MPA-JHU catalog were derived by using the median instrumental resolution, which will introduce redshift-dependent bias as the true instrumental resolution is a function of the wavelength. The spectrum and associated wavelength-dependent instrumental resolution of each object were available in the SDSS archive². The fitting was done using the pPXF code (Cappellari 2017) by adopting the HR-PYPOPSTAR theoretical stellar populations with 50,000 resolving power at 5000Å (Millán-Irigoyen et al. 2021). During the fitting, we further exclude 5800-6100Å range where blue and red channels of the spectrograph with different instrumental resolutions overlap. The derived velocity dispersion within a 3'' fiber was then corrected to that at PETROR50_R by the following equation (Cappellari et al. 2006):

$$\sigma_e = \sigma_{\text{fiber}} (R_e / R_{\text{fiber}})^{0.066 \pm 0.035}. \quad (4)$$

Here the error on the power-law index is implemented through `numpy.random.normal`.

¹ <https://www.mpa.mpa-garching.mpg.de/SDSS/DR7/>

² <http://data.sdss.org/sas/dr12/sdss/spectro/redux/26/spectra/>

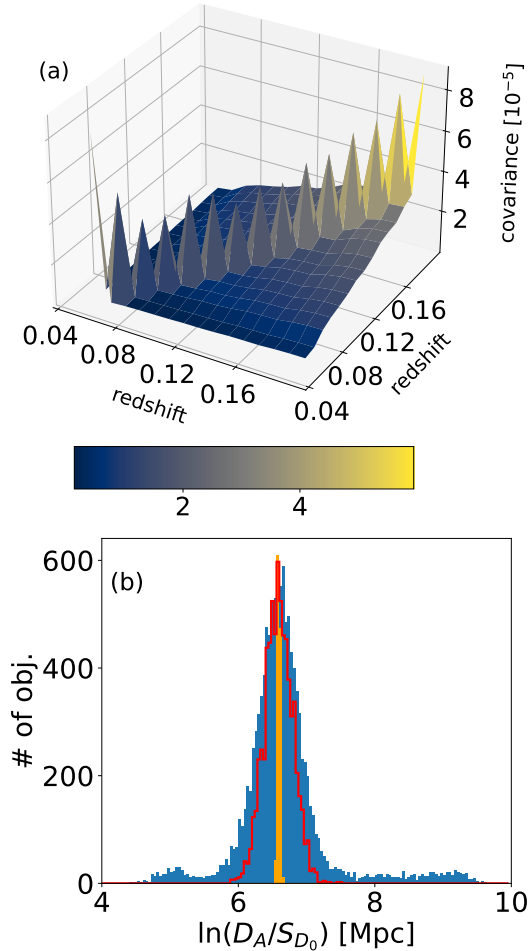


Figure 3. (a) The covariance matrix of the distance measurements at different redshift bins. (b) The distribution of the derived angular diameter distances of elliptical galaxies in the SDSS main galaxy sample (blue filled) within the redshift bin of $[0.17, 0.18]$. The red open histogram shows the simulated distributions based on the median errors of three observables in the galaxy catalog, and the orange filled histogram is the simulation that only considers the observed redshift distribution plus random peculiar velocities of 1000 km/s (orange filled). Note that the two simulated distributions are rescaled to have the same median and histogram peak as the observed one.

5 THE DISTANCE VS. REDSHIFT DIAGRAM OF THE SDSS ELLIPTICAL SAMPLE.

The redshift distribution of the SDSS elliptical sample peaks around 0.11. We limit the redshift range to $[0.05, 0.2]$ and construct the distance vs. redshift diagram with a redshift bin size of 0.01. The number of galaxies in individual redshift bins result in negligible fractional errors of their median redshift, which is $< 0.06\%$ for a random peculiar velocity of 1000 km/s. The upper range at $z=0.2$ is also necessary to avoid the Malmquist bias caused by the magnitude cut of $r < 17.77$. Although the massE ruler is not subject to the sample completeness, objects that are selected into the sample can systematically bias the stellar mass if their luminosity is overestimated due to the Malmquist bias. To estimate it roughly, we use the r -band luminosity function (Blanton et al. 2003) to construct a mock r -band photometric sample down to the SDSS $5\text{-}\sigma$ depth ($r=22.7$) at different redshifts, and add the photometric error based on the me-

Table 1. The angular diameter distance as derived by the massE ruler.

ID	z_{med}	$\ln(D_A(z_{\text{med}})/S_{D_0})$
<hr/>		
ln(Mpc)		
1	0.0549	5.5840
2	0.0652	5.7371
3	0.0752	5.8830
4	0.0847	5.9884
5	0.0950	6.0851
6	0.1051	6.1746
7	0.1150	6.2391
8	0.1251	6.2892
9	0.1348	6.3628
10	0.1449	6.4589
11	0.1546	6.5070
12	0.1649	6.5449
13	0.1749	6.6054
14	0.1846	6.6676
15	0.1948	6.6847

dian and standard deviation of apparent magnitude errors as a function of magnitude from the SDSS sample. By assuming a constant mass-to-light ratio in the r -band, it is found that the median distance is under-estimated by 1% at $(z, \Delta z) = (0.2, 0.01)$ while by as much as 7% at $(z, \Delta z) = (0.25, 0.01)$ for the sub-sample with $r < 17.77$. As a result, we limit the z range to be below 0.2 so that the Malmquist bias is a small fraction of the typical $1\text{-}\sigma$ uncertainty in individual redshift bins that are around 1.3% including both observational errors and systematic errors in β (see § 6.2).

As stated above, the massE ruler has two nuisance parameters: S_{D_0} calibrates the absolute distance, which degenerates with the local Hubble constant, and β determines the relative distances among galaxies with different masses. The latter is transformed to the curvature of the distance-redshift diagram, because for a flux limited sample galaxies at higher redshifts have higher masses. The massE ruler would be a viable new probe of cosmic expansion history, only if for a fixed β the massE ruler gives a smooth function of the distance vs. redshift with small fluctuations, otherwise systematic errors unrelated to β , e.g., some hidden parameters, may be too large for the massE ruler to be feasible. The latter is in fact the case for other galaxy scaling laws. As a sanity check, we let β uniformly distribute over a very large range from 0 to 1, and carry out the fitting with flat Λ CDM through *cosmosis* (Zuntz et al. 2015) and *emcee* sampler (Foreman-Mackey et al. 2013). As listed in Table 3, Ω_Λ converges to be a reasonable value, i.e., 0.54 ± 0.28 , along with $\beta = 0.41 \pm 0.09$. This indicates that once β is estimated from the local relationship, the performance of the massE ruler can further improve.

Figure 2 (a) shows the derived distance-redshift diagram in terms of $\ln(D_A/S_{D_0})$ as a function of redshift, which is also listed in Table 1. As shown in Figure 3 (a) and listed in Table 2, the covariance matrix of $\ln(D_A/S_{D_0})$ includes two parts. The first one is caused by the observational errors of σ_e , $R_{e,as}$ and M_{star} . In the case of no observational errors, the derived D_A distribution should be the redshift distribution convolved with peculiar velocity. As an example shown in Figure 3 (b) for $z=[0.17, 0.18]$, the derived $\ln(D_A)$ distribution (blue filled) scatters much more broadly than that implied by the redshift distribution (orange filled). The distribution can be approximated with a central Gaussian core plus a broad wing. The standard deviation of the central core is 0.29, which is consistent with but slightly larger than the square root of the quadratic sum of quoted median errors of three observables in the catalog (red open symbols)

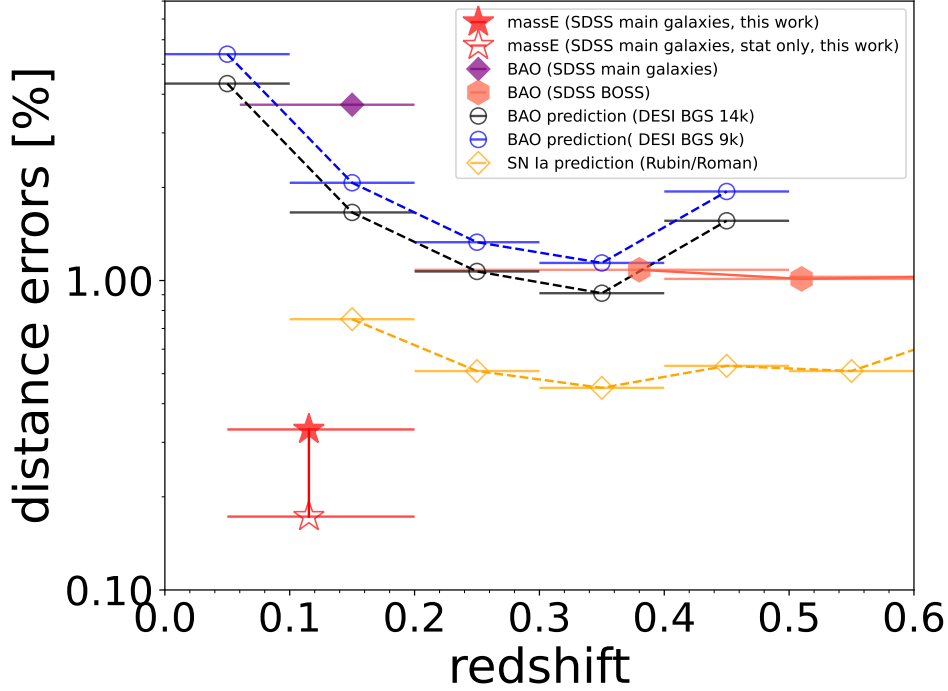


Figure 4. The fractional errors of distance measurements at different redshifts by different methods, including massE with SDSS main galaxies (this work), BAO with SDSS main galaxy survey (MGS) (Ross et al. 2015), BAO with SDSS BOSS data (Alam et al. 2017), BAO prediction with DESI (DESI Collaboration et al. 2016) and SN Ia prediction with Rubin/Roman (Feng et al. 2014).

Table 2. The covariance matrix of the angular diameter distance $\ln(D_A(z_{\text{med}})/S_{D_0})$.

82.38	0.49	0.83	0.96	1.24	1.45	1.64	1.79	2.01	2.34	2.49	2.69	3.01	3.16	3.27
0.49	51.29	1.28	1.47	1.88	2.23	2.48	2.71	3.01	3.52	3.72	3.96	4.47	4.69	4.87
0.83	1.28	36.32	2.48	3.20	3.76	4.22	4.62	5.18	6.05	6.42	6.92	7.77	8.12	8.44
0.96	1.47	2.48	36.24	3.75	4.40	4.93	5.41	6.05	7.08	7.52	8.13	9.10	9.49	9.88
1.24	1.88	3.20	3.75	45.49	5.69	6.38	7.00	7.84	9.16	9.73	10.53	11.80	12.30	12.80
1.45	2.23	3.76	4.40	5.69	45.02	7.49	8.21	9.20	10.76	11.41	12.34	13.85	14.44	15.02
1.64	2.48	4.22	4.93	6.38	7.49	37.99	9.21	10.32	12.06	12.80	13.85	15.53	16.20	16.85
1.79	2.71	4.62	5.41	7.00	8.21	9.21	45.24	11.34	13.25	14.07	15.22	17.07	17.80	18.51
2.01	3.01	5.18	6.05	7.84	9.20	10.32	11.34	45.28	14.86	15.79	17.10	19.17	19.99	20.79
2.34	3.52	6.05	7.08	9.16	10.76	12.06	13.25	14.86	53.22	18.44	19.98	22.40	23.36	24.29
2.49	3.72	6.42	7.52	9.73	11.41	12.80	14.07	15.79	18.44	55.99	21.24	23.79	24.81	25.81
2.69	3.96	6.92	8.13	10.53	12.34	13.85	15.22	17.10	19.98	21.24	67.13	25.81	26.89	27.98
3.01	4.47	7.77	9.10	11.80	13.85	15.53	17.07	19.17	22.40	23.79	25.81	70.35	30.15	31.36
3.16	4.69	8.12	9.49	12.30	14.44	16.20	17.80	19.99	23.36	24.81	26.89	30.15	79.61	32.69
3.27	4.87	8.44	9.88	12.80	15.02	16.85	18.51	20.79	24.29	25.81	27.98	31.36	32.69	88.80

All numbers are in $10^{-6} \ln(\text{Mpc})^2$. Each number gives the covariance between i -th and j -th redshift bins as listed in Table 1.

through Equation 2, which gives 0.21. This indicates that the quoted errors of observables are slightly under-estimated. The broad wing is due to outliers of measurements. As a result, we adopt the standard deviation of the whole distribution divided by the square root of the number of objects as the error. It is about two times larger than the one derived by the bootstrap method. Since each redshift bin is independent, all non-diagonal elements of the covariance matrix are set to zero for this first part. The second part is due to the variation in β . We adopt its measurement and associated error from the local sample to calculate the corresponding covariance matrix of $\ln(D_A/S_{D_0})$. Note that all uncertainties, e.g., the systematic uncertainties in the stellar initial mass function, which shifts all distances by the same amount, are taken into account by S_{D_0} .

6 CONSTRAINTS ON COSMOLOGICAL PARAMETERS

6.1 Constraints on the flat Λ CDM

We carry out the fitting to the distance vs. redshift diagram in Figure 2 as obtained by the massE ruler with a flat Λ CDM. The fitting was done through *cosmosis* (Zuntz et al. 2015) with the emcee sampler (Foreman-Mackey et al. 2013), whose priors are listed in Table A1 where both h_0 and S_{D_0} are set to be free. As shown in Figure 2 (c), the convergent results have $\Omega_\Lambda=0.675\pm 0.079$, which is $1-\sigma$ consistent with constraints by BAO (Ross et al. 2015; Alam et al. 2017), SN Ia (Scolnic et al. 2018) and CMB (Planck Collaboration et al. 2020). The massE ruler thus proves the acceleration

Table 3. The best-fit cosmological parameters.

β priors [†]	M_{star} for massE	rulers	β	Ω_{DE}	w
flat Λ CDM					
U(0, 1)	MPA-JHU	massE	0.41 ± 0.09	0.54 ± 0.28	–
fixed to N (0.4036 \pm 0.0016)	MPA-JHU	massE	–	0.675 ± 0.079	–
fixed to N (0.4036 \pm 0.0016)	CIGALE	massE	–	0.678 ± 0.078	–
flat w CDM					
		SN Ia	–	$0.68^{+0.07}_{-0.08}$	$-1.06^{+0.23}_{-0.19}$
		BAO	–	$0.72^{+0.02}_{-0.03}$	$-0.73^{+0.17}_{-0.16}$
		CMB	–	$0.80^{+0.06}_{-0.03}$	$-1.49^{+0.26}_{-0.31}$
		massE	–	$0.67^{+0.27}_{-0.17}$	$-0.97^{+0.42}_{-0.30}$

[†]U stands for a uniform distribution and N is for a normal distribution. All other priors are included in Table A1.

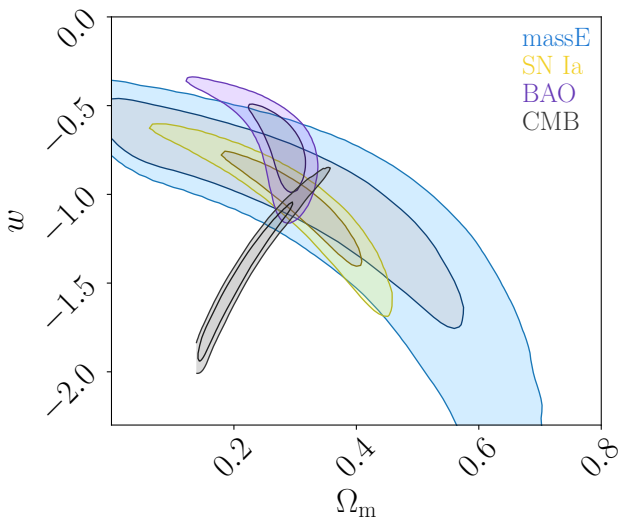


Figure 5. The confidence range of the dark energy equation of state (w) and the dark matter density (Ω_{m}) for the flat w CDM model by CMB, BAO, SN Ia and massE, respectively. The lower-left cut for the CMB is caused by the H_0 prior that is set to be < 100 km/s/Mpc. The plot was produced through ChainConsumer (Hinton 2016).

of the universe at $8.5\text{-}\sigma$ with elliptical galaxies in the SDSS main galaxy sample under flat Λ CDM.

Among three observables, $M_{\text{star},1\text{Mpc}}$ relies on the stellar population synthetic model, while the other two are straightforward measurements with weak model dependence. We thus carry out additional sets of stellar mass measurements and compared to the result of the MPA-JHU catalog. It is found that with multi-band broad SED, the systematic effect of M_{star} measurements on the derived cosmological parameters is small as long as the parameter space of the population synthetic model is reasonably sampled. We use CIGALE (Boquien et al. 2019) to construct a two exponential decaying star formation history with the second one for the late-epoch burst. The fraction of models that experiences late bursts is 20%, smaller than 50% in MPA-JHU (Kauffmann et al. 2003). The metallicity is uniformly distributed among four discrete values that are 0.2, 0.4, 1.0 and 2.5 solar, while in MPA-JHU the metallicity is interpolated to a higher resolution. The interstellar medium extinction is uniform between 0.0 and 1.5, while the MPA-JHU catalog extends to higher

values. Although the standard deviation of the difference between MPA-JHU’ and CIGALE’ stellar masses reaches 20%, the systematic offset is much smaller. As listed in Table 3, the best-fit Ω_{Λ} is 0.678 ± 0.078 for the flat Λ CDM, which is essentially the same as the one (0.675 ± 0.079) with the MPA-JHU mass.

6.2 The statistical power in distance measure

To illustrate the statistical advantage in distance measure with the massE ruler, Figure 4 compares the fractional error of the massE-based distance to those by SN Ia and BAO. We sum the covariance matrix to obtain this error. In our redshift range of [0.05, 0.2] with a median redshift $z_{\text{med}}=0.11$, the corresponding angular diameter distance is $\ln(D_{\Lambda}(z_{\text{med}})/S_{D_0}[\text{Mpc}])=6.1987 \pm 0.0034$. This fractional distance error of 0.34% is a quadratic sum of 0.17% by errors of three observables and 0.3% by β uncertainties. A double check of this estimate can be obtained by looking at the residual of the best fit as shown in Figure 2 (b). For each bin, the deviation from the true distance is caused by the statistical error of three observables plus one realization of the intrinsic massE relationship that is independent from other bins. As a result, the fluctuation in the residual should converge to the result by the covariance matrix if the number of redshift bins is large enough. An error of 0.35% is derived from the standard deviation of the residual for the median distance of the above redshift range, which is close to the one from the covariance matrix. We further check whether the Malmquist bias can affect this error estimate by calculating the bias for each redshift bin and treating it as additional independent error. It is found that the final fractional distance error increases negligibly from 0.35% to 0.36%.

As shown in the figure, the measurement with massE gives about one order of magnitude smaller fractional errors than existing measurements at similar redshift with SN Ia and BAO (Ross et al. 2015; Alam et al. 2017; Scolnic et al. 2018). As compared to next-generation surveys as offered by BAO from DESI and SN Ia from Rubin/Roman (Feng et al. 2014; DESI Collaboration et al. 2016), the massE ruler still offers 2–4 times smaller fractional error at $z \sim 0.1$. This demonstrates the statistical power of the massE ruler as a new probe of cosmic geometry.

The statistical power of the massE ruler can be understood in the following way. Although each SN Ia offers a fractional distance error of $\sim 5\%$ as compared to $\sim 25\%$ of the massE, the number of elliptical galaxies is far more numerous than the SN Ia. On the other hand, BAO is essentially volume-limited at low- z .

6.3 Constraints on the dark energy equation of state CDM (w CDM)

The low- z distance measurements at high accuracy by massE is particularly useful to probe the deviation from the constant of the dark energy density that dominates at the low- z universe. As shown in Figure 5, we illustrate this by carrying out constraints on the w CDM model with the massE data and compare to those with the Pantheon SN Ia data (Scolnic et al. 2018), the MGS/BOSS/eBOSS BAO data (Ross et al. 2015; Alam et al. 2017, 2021) and the Planck 2018 CMB TT,TE,EE+lowE data (Planck Collaboration et al. 2020), respectively. All fittings have been done with *cosmosis* (Zuntz et al. 2015) and *emcee* sampler (Foreman-Mackey et al. 2013). As listed in Table 3, the massE alone constrains w to an error that is only a factor of 2.2, 1.7 and 1.3 larger than the current one by BAO only, SN Ia only and CMB only, respectively.

7 CONCLUSION

In this study we have shown that the massE relationship of galaxies could be a new cosmic ruler to probe the distance-redshift diagram with advantage of its statistical power. It has two nuisance parameters with three observables for ellipticals that are galaxy sizes, velocity dispersions and stellar masses. With the SDSS MGS sample, the distance at $z=0.11$ with the massE ruler is constrained to a fractional error of 0.34%, with the best-fit dark energy density of 0.675 ± 0.079 for flat Λ CDM. In principle the massE can be applied to higher z by combining large-area space-based imaging survey and ground-based deep spectroscopic survey.

The *cosmosis* modules including the input parameter files and data files for the massE can be obtained through the link available on arXiv of this manuscript.

ACKNOWLEDGEMENTS

We thank the referee for constructive comments that help improve the paper. We thank Pengjie Zhang for helpful comments. Y.S. acknowledges the support from the National Key Research and Development Program of China (No. 2018YFA0404502), the National Natural Science Foundation of China (NSFC grants 11825302, 12141301, 12121003, 11733002), the science research grants from the China Manned Space Project with NO. CMS-CSST-2021-B02, and the Tencent Foundation through the XPLORER PRIZE. S.M. is partly supported by the National Key Research and Development Program of China (No. 2018YFA0404501), by the National Natural Science Foundation of China (11821303, 11761131004 and 11761141012) and by Tsinghua University Initiative Scientific Research Program ID 2019Z07L02017. Z.Y.Z acknowledges the support of the National Natural Science Foundation of China (NSFC) under grants No. 12041305, 12173016, the Program for Innovative Talents, Entrepreneur in Jiangsu, and the science research grants from the China Manned Space Project with NO. CMS-CSST-2021-A08, CMS-CSST-2021-A07.

Funding for the SDSS and SDSS-II has been provided by the Alfred P. Sloan Foundation, the Participating Institutions, the National Science Foundation, the U.S. Department of Energy, the National Aeronautics and Space Administration, the Japanese Monbukagakusho, the Max Planck Society, and the Higher Education Funding Council for England. The SDSS Web Site is <http://www.sdss.org/>. The SDSS is managed by the Astrophysical Research Consortium for the Participating Institutions. The Participating Institutions are

the American Museum of Natural History, Astrophysical Institute Potsdam, University of Basel, University of Cambridge, Case Western Reserve University, University of Chicago, Drexel University, Fermilab, the Institute for Advanced Study, the Japan Participation Group, Johns Hopkins University, the Joint Institute for Nuclear Astrophysics, the Kavli Institute for Particle Astrophysics and Cosmology, the Korean Scientist Group, the Chinese Academy of Sciences (LAMOST), Los Alamos National Laboratory, the Max-Planck-Institute for Astronomy (MPIA), the Max-Planck-Institute for Astrophysics (MPA), New Mexico State University, Ohio State University, University of Pittsburgh, University of Portsmouth, Princeton University, the United States Naval Observatory, and the University of Washington.

DATA AVAILABILITY

All the data used here are available upon reasonable request.

REFERENCES

- Alam S., et al., 2017, *MNRAS*, **470**, 2617
 Alam S., et al., 2021, *Phys. Rev. D*, **103**, 083533
 Bernardi M., et al., 2003, *AJ*, **125**, 1866
 Blanton M. R., et al., 2001, *AJ*, **121**, 2358
 Blanton M. R., et al., 2003, *ApJ*, **592**, 819
 Boquien M., Burgarella D., Roehly Y., Buat V., Ciesla L., Corre D., Inoue A. K., Salas H., 2019, *A&A*, **622**, A103
 Brinchmann J., Charlot S., White S. D. M., Tremonti C., Kauffmann G., Heckman T., Brinkmann J., 2004, *MNRAS*, **351**, 1151
 Cappellari M., 2017, *MNRAS*, **466**, 798
 Cappellari M., et al., 2006, *MNRAS*, **366**, 1126
 DESI Collaboration et al., 2016, arXiv e-prints, p. arXiv:1611.00036
 Eisenstein D. J., et al., 2005, *ApJ*, **633**, 560
 Feng J. L., et al., 2014, arXiv e-prints, p. arXiv:1401.6085
 Foreman-Mackey D., Hogg D. W., Lang D., Goodman J., 2013, *PASP*, **125**, 306
 Hinton S. R., 2016, *The Journal of Open Source Software*, **1**, 00045
 Howlett C., Said K., Lucey J. R., Colless M., Qin F., Lai Y., Tully R. B., Davis T. M., 2022, arXiv e-prints, p. arXiv:2201.03112
 Hubble E., 1929, *Proceedings of the National Academy of Science*, **15**, 168
 Kauffmann G., et al., 2003, *MNRAS*, **341**, 33
 Law D. R., et al., 2021, *AJ*, **161**, 52
 Lemaître G., 1927, *Annales de la Sociéteété Scientifique de Bruxelles*, **47**, 49
 Magoulas C., et al., 2012, *MNRAS*, **427**, 245
 Millán-Irigoyen I., Mollá M., Cerviño M., Ascasibar Y., García-Vargas M. L., Coelho P. R. T., 2021, *MNRAS*, **506**, 4781
 Perlmutter S., et al., 1999, *ApJ*, **517**, 565
 Planck Collaboration et al., 2020, *A&A*, **641**, A6
 Riess A. G., et al., 1998, *AJ*, **116**, 1009
 Ross A. J., Samushia L., Howlett C., Percival W. J., Burden A., Manera M., 2015, *MNRAS*, **449**, 835
 Salvatier J., Wiecki T. V., Fonnesbeck C., 2016, PyMC3: Python probabilistic programming framework (ascl:1610.016)
 Scolnic D. M., et al., 2018, *ApJ*, **859**, 101
 Shi Y., Yu X., Mao S., Gu Q., Xia X., Chen Y., 2021, *MNRAS*, **507**, 2423
 Zuntz J., et al., 2015, *Astronomy and Computing*, **12**, 45

APPENDIX A: PRIORS OF COSMOLOGICAL PARAMETERS

The priors of cosmological parameters are detailed in Table A1. All fittings have been done with *cosmosis* (Zuntz et al. 2015) and *em-*

Table A1. Priors of cosmological parameters.

parameters	priors	models
massE only		
Ω_m	U(0.0, 1.0)	flat Λ CDM, flat wCMD
h_0	U(0.2, 1.0)	flat Λ CDM, flat wCMD
S_{D_o}	U(0.3, 2.0)	flat Λ CDM, flat wCMD
w	U(-3.0, 0.0)	flat wCMD
SN Ia only		
Ω_m	U(0.0, 1.0)	flat wCMD
h_0	U(0.2, 1.0)	flat wCMD
M	U(-23, -15)	flat wCMD
w	U(-3.0, 0.0)	flat wCMD
BAO only		
Ω_m	U(0.0, 1.0)	flat wCMD
h_0	U(0.2, 1.0)	flat wCMD
Ω_b	U(0.001, 0.3)	flat wCMD
w	U(-3.0, 0.0)	flat wCMD
CMB only		
Ω_c	U(0.0, 0.9)	flat wCMD
Ω_b	U(0.0, 0.3)	flat wCMD
h_0	U(0.2, 1.0)	flat wCMD
w	U(-3.0, 0.0)	flat wCMD
n_s	U(0.8, 1.2)	flat wCMD
$10^9 A_s$	U(1.48, 5.45)	flat wCMD
k_s	0.05	flat wCMD
τ	U(0.01, 0.8)	flat wCMD

U stands for a uniform distribution.

cee sampler (Foreman-Mackey et al. 2013). Each fitting has 4×10^6 samples, with the Gelman-Rubin (G-R) convergence value of < 0.01 , except for CMB that has 15×10^6 samples in order to have G-R value below 0.01.

This paper has been typeset from a $\text{\TeX}/\text{\LaTeX}$ file prepared by the author.